Coherent single Erbium spin qubit manipulation at milli-Kelvin temperature

Yuxiang Pei 12249599

University of Chicago, Physical Sciences Department

Overview: Quantum technologies have drawn great attention from researchers and companies recently. Towards the aim of high-fidelity quantum computation and scalable quantum networks, spins are playing the role of basic building blocks. Therefore, it is of essential importance to achieve coherent control and manipulation of single spin. Optical addressing of single REI [1] and proposals for detecting a single electron spin in a microwave resonator [2] have already rised up. Erbium spin-based quantum systems are an emerging candidate for quantum memory [3] as well as quantum transducers [4]. Due to their long coherence time and large, anisotropic g-Factor, rare-earth ions (REIs) in crystals enable a hybrid quantum information processing architecture by interfacing these rare-earth based technologies with superconducting devices.

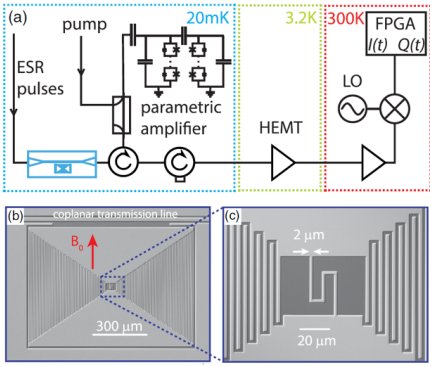

Figure 1: **Prior art on mk ESR device and setup [5].** (a) Schematic of the experimental setup. The output field of the resonator is amplified by a JPA at base temperature, further amplified by a high-electron mobility transistor (HEMT) amplifier at 3.2 K and demodulated with an IQ mixer at room temperature to record and process the quadratures of the signal with FPGA electronics. (b) Optical micrograph of a planar superconducting resonator with low characteristic impedance $Z \approx 8\ \Omega$ that is side coupled to a coplanar transmission line for control and read-out. Coupling between the spins and the resonator field occurs below the inductive wire shown in (c).

Objective: Achieving single spin coupling at cryogenic temperature by enhancing the sensitivity of spectrometer. Perform single spin detection and manipulation through coherent/incoherent readout, optical drive and control.
Here we propose the development of on-chip planar superconducting resonators which could serve as the high-sensitivity spectrometer for detecting single spins. The basic idea is to design a loop-gap type resonator on top of

an Er^{3+} doped Yttrium oxide thin film epitaxially grown on silicon substrate, which could perform single spin Electron Spin Resonance (ESR) at milli-Kelvin temperatures achieved using Dilution refrigerator-based systems. By enhancing the capacitance and reducing the inductance of the superconducting resonator, we expect to achieve a smaller characteristic impedance of this device, which will lead to a larger current flowing through the wire. This would enhance the magnetic field within the mode volume and directly give us a larger coupling.
Methods and timeline: I will first design and simulate different kinds of planar superconducting resonators using Ansys EM software and try to figure out the maximum coupling. Then I would figure out effective detection methods that could resolute the signal of single spin. Ultimately, we will fabricate the device and put into real experiments, and used in more exciting applications.

1 Introduction

1.1 Rare earth ions

Rare-earth ions (REIs) in crystals are promising candidate systems for quantum information applications. Inside the chemically active $6s$ and $5d$ electrons, the rare-earth ions have a full $5s^2 5p^6$ shell shielding a partially filled $4f$-subshell. This structure brings with REIs the weak interaction with environment, which enables them to behave like free ions even when doped into solid state hosts. Rare-earth ions in dielectric crystals at low temperature provide a combination of long optical and spinstate coherence times as well as the possibility of controlling linebroadening and interactions by external electric and magneticfields; these properties make them ideally suited for quantum information processing. [6]

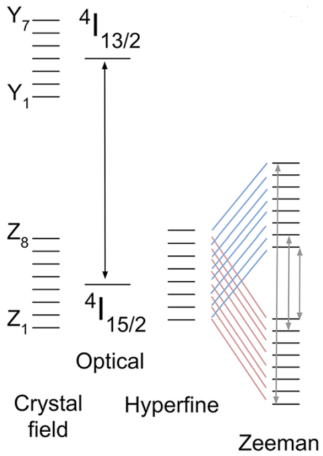

Figure 2: **Energy level diagram of $Er^{3+} : Y_2O_3$ [7].** A schematic of the energy levels of interest in the Er^{3+} Stark levels from the crystal field effect and the Zeeman splitting of the hyperfine levels which is seen in EPR.

Among the REIs, yttrium oxides are good candidates because oxygen has zero spin and yttrium has a low magnetic moment [8]. As is shown in Fig 2, the crystal field effect breaks the spherical symmetry of the free ion, and this results in the splitting of the ground state ($^4I_{15/2}$) into 8 Stark levels and the first excited state ($^4I_{13/2}$) into 7 Stark

levels. The energy levels that are degenerate for free ions would be further splitted by crystal field and external magnetic field, the splitting is often in the range of a few MHz up to a few GHz, which enables us to couple the transition between Zeeman splitting levels to a microwave field. In erbium doped yttrium oxide, erbium ions offer a unique opportunity of a coherent conversion of microwave photons into the telecom C band at 1.54 μm, which is used for long distance fiber-optical communication [9].
Furthermore, rare earth spins have been demonstrated to exhibit an order of magnitude increase in spin lifetime T_1 as well as coherence time T_2 at milli-Kelvin temperatures from 4 Kelvin [10] [11]. Hence, milli-Kelvin temperatures offer an ideal regime for high coherence operation of Erbium spin qubits. In recent years,

1.2 Spin dynamics in a classical microwave field

Consider an electronic spin-1/2, submitted to a classical magnetic field $B(t)$. The two systems interact via the Hamiltonian $H = -\mu \cdot B(t)$. When a static field $B_0 = B_0 e_z$ is applied, the magnetization vector precesses around B_0 at frequency ws, the so-called Larmor frequency.
Consider next the application of an oscillating microwave field $B_1(t) = 2cos(wt)B_1 e_x$ orthogonal to B_0. Under this drive, the magnetization vector M rotates around a vector in rotating frame $\omega_1 \widetilde{e}_x + \Delta_s e_z$ at an angular speed called the Rabi frequency [12]

$$\Omega_R = \sqrt{\Delta_s^2 + \omega_1^2} \tag{1}$$

Where $\Delta_s = \omega - \omega_s$ is the frequency difference between Lamor frequency and rotating frame, ω_1 is the corresponding Larmor frequency of B_1. By applying a microwave pulse, the Bloch vector could be rotated by an angle depending on the pulse length. Such a control allows to bring the magnetization vector to every point of the Bloch sphere.
We know that the isolated spin-1/2 systems undergoes a constant precession. The consistent Rabi frequency ensures a relative phase of spins and is the source of **coherence**, which is of central importance in quantum computation. In real systems, however, under the environmental influence, the relative phase might be undermined and become totally random. The time it takes for a single spin to completely lose its direction is called decoherence time T_2. There also exists spin-environment coupling which causes a spin in the upper energy level to jump to the lower level. The average transition time is defined as relaxation time T_1. Both T_1 and T_2 are important parameters for judging the quality of qubits. The decoherence of an ensemble of spins rather than a single spin is noted as

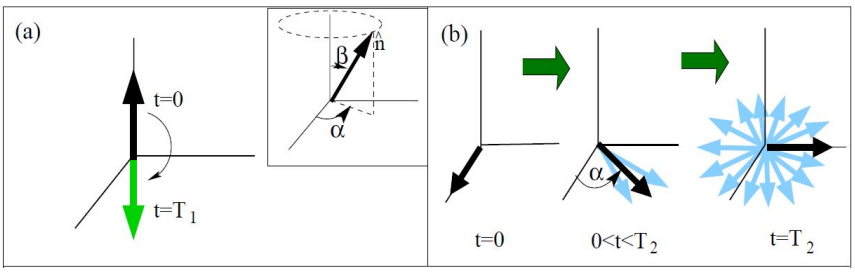

Figure 3: **An illustration of T_1, T_2 [13].** (a) Relaxation time T_1: average transition time from upper level to lower level. (b) The precession of spin in xy-plane, and decoherence after irregular precession.

T_2*. In addition to the uncertainty in the precession angle of a single spin at a given time, there will be an uncertainty in the relative precession angles among different spins due to the spatial inhomogeneity. This additional decoherence source leads normally to T_2*< T_2. The ensemble relaxation time T_1* is proved to be fundamentally different from T_1, as is illustrated in Fig 3. All spins are initially in their upper levels. Due to the random coupling strength for different spins, their Rabi frequencies are also random, and spins initially in phase will be out of phase during the evolution. We could find the polarization of the system relaxes after a characteristic time T_1* as is shown in the inset.

1.3 Spin Echo

In magnetic resonance, a spin echo is the refocusing of spin magnetisation by a pulse of resonant electromagnetic radiation. Spin magnetisation is measured through the coupling to system, typically the coupling of an ensemble of spins to a cavity mode or a resonator field. The spins could be the outer electron spins of molecules/ions in electron paramagnetic resonance (EPR) and spins of individual donors/electrons in electron spin resonance (ESR) measurements, or even spin of nuclei in nuclear magnetic resonance (NMR) measurements. They form spin-1/2 systems under applied magnetic fields.
At first, the spins are statistically aligned in a constant applied magnetic field. Viewed from the rotating frame, the magnetization components precessing at Larmor frequency will appear stationary. The specifically designed devices, for example a carefully fabricated superconducting cavity, enables us to apply another oscillating magnetic field perpendicular to the original field. This magnetic field will rotate the magnetization about the external external field, and the rotated angle is called tip angle.

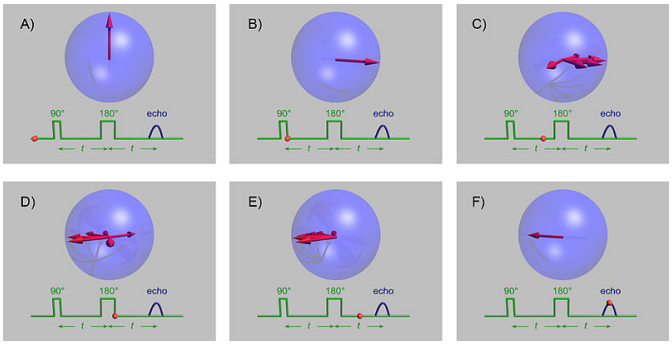

Figure 4: **Spin echo animation showing the response of spins (red arrows) in the blue Bloch sphere to the green pulse sequence** [14]**.** A) Illustration is in a rotating reference frame where the spins are stationary on average. B) 90°pulse has been applied that flips the arrow. C) Signal decay. D) A 180 degree pulse is now applied so that the rotation is reversed. E) Evolution of moment. F) Complete refocusing has occurred and at this time, an accurate T_2 echo can be measured with all T_2* effects removed.

After an excitation pulse is applied, magnetic signal follows a decay with time due to both spin relaxation and any inhomogeneous effects. Spin relaxation leads to an irreversible loss of magnetisation. However, the inhomogeneous dephasing can be removed by applying a 180°pulse that inverts the magnetisation. If the inversion pulse is applied after a period t of dephasing, the inhomogeneous evolution will rephase to form an echo at 2t.
We could deduce the number of T_2 from the intensity of echoes relative to initial signals. T_2* could be approximated by the duration of echo. For the T_1 measurement, by sending

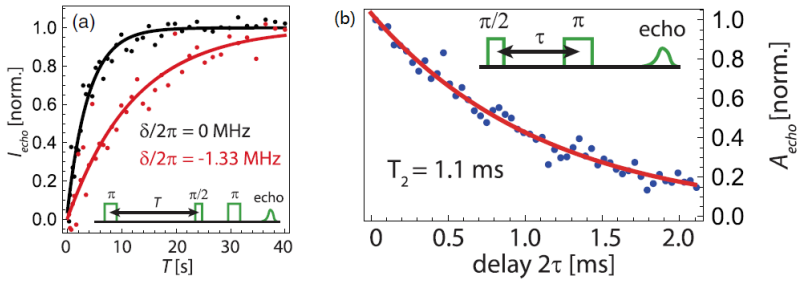

Figure 5: **Coherence measurement of phosphorus donors [5].** (a) Measurement of T_1 as a function of frequency detuning. (b) Measurement of T_2 fitted by an exponential decay time.

an initial π pulse which inverts the spin population. After a variable time T the recovery of the spin population is probed with a standard Hahn echo sequence to determine what fraction of the spins have relaxed back to the ground state. The spin population is fitted by an exponential function from which we extract the spin T_1. By far, T_1, T_2 and T_2* could be measured experimentally. Fig 5 presents the measured data of phosphorus donors localized in a 200 μm^2 area through ESR.

1.4 Basic principles of ESR

The Electron Spin Resonance (ESR) is a useful technique in characterizing the spin energy levels as well as the coherence time of paramagnetic ions.
Consider an ensemble of N spins coupled to a resonator of frequency w_0 with identical coupling constant g, and the resonator is coupled to input and output transmission lines. As is shown in Fig 6. The spins are probed by a Hahn-echo sequence sent via port 1 that ultimately triggers the emission of an echo. We make the assumption that the spins-resonator system is in the weak-cooperativity regime and we neglect transverse relaxation. The spin ensemble will evolute from an equilibrium polarization along the z-direction, then an ideal $\pi/2$ pulse around the x-axis creates a transversal magnetization state. Due to the spin ensemble inhomogeneity, the transverse magnetization decays in a time $1/\omega$.

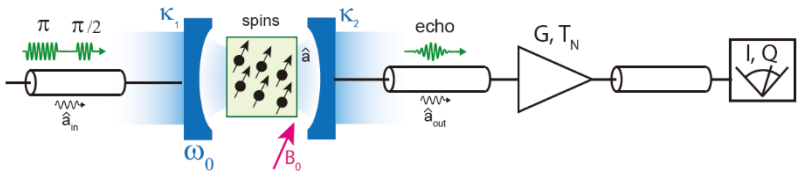

Figure 6: **ESR setup [12].** A train of microwave pulses triggers the emission of an echo by the spins.

After brief calculation we know that the output signal is emitted on the quadrature at resonance. The echo is mainly emitted into the detection waveguide before being amplified and detected via a homodyne setup that yields the quadratures I and Q of the signal. The sensitivity of the experiment can be defined as the number of spins detectable in a single-echo with a signal-to-noise ratio of 1.

1.5 Proposal for single spin sensitivity

Important progress in ESR sensitivity has been made by inductively coupling spins to superconducting resonators through the magnetic dipole interaction and by adopting ideas and techniques from circuit quantum electrodynamics [5] [15]. There's also been significant progresses in hybrid quantum systems, combining the long coherence of natural quantum systems and the strong coupling to EM fields of artificial quantum systems (superconducting qubits) [16].
For a nano-fabricated LC resonator, the circuit inductance, through which flows a current δI, generates an oscillating magnetic field $\delta \boldsymbol{B}$ at the spin location. The spin-resonator coupling is given by:

$$g = \gamma_e |\langle e|\delta \boldsymbol{B}(r) \cdot \boldsymbol{S}|g\rangle| \tag{2}$$

where |e> and |g> are the energy levels spanning the ESR transition to be probed. We have

$$\delta \boldsymbol{I} = \omega_0 \sqrt{\hbar / 2Z_0} \tag{3}$$

Z_0 being the resonator impedance. Maximizing g thus requires minimizing Z_0 and bringing the spins as close as possible to the inductance.
To achieve small mode volume and low loss, the state of art is to fabricate on-chip superconducting resonators [17]. For that $Z_0 = \sqrt{(L/C)}$, the key is to generate large capacitance and small inductance. We implement a lumped-element geometry, combining a small inductor loop patterned in parallel with large interdigitated capacitors. We carry on simulations to find out a design which could confine the largest oscillating magnetic field in the loop, thus maximize g and calculate sensitivity. If a rare earth ion doped in crystal happens to lie within this loop, it could be addressed, manipulated and read out via magnetic dipole coupling with our device.

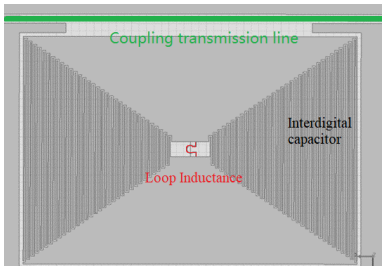

Figure 7: **Illustration of device.** A transmission line (green) couples microwave to the LC resonator (red and black).

2 Simulation results

2.1 Loop design

I applied $AnsysEM19.0$ software to load the device geometry: superconducting patterns on a $3.4 \times 2.5 \times 0.35$ μm silicon substrate. The patterns' boundary conditions are set as perfect conductors and microwave power is sent through both ports of the transmission line.
From the field distribution we know that on resonance (5.95 GHz), the magnetic current is strongest in the loop, thus magnetic field induced by this current is mostly confined

within the loop. After plotting out the field, we get close to 5.48 nT in the center of the loop. Simulation also shows that with a loss tangent of 10^{-4} for the silicon substrate, quality factor Q is around 1.1×10^4.

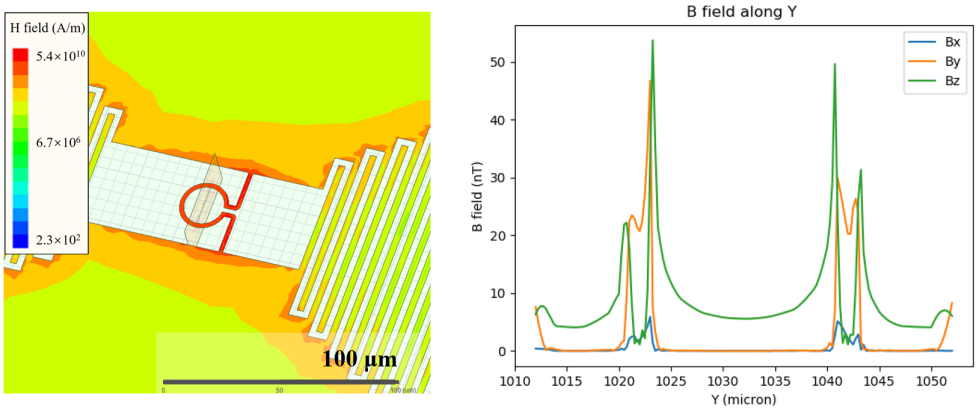

Figure 8: **H field on resonance.** Geometry, and cross-section of B field along y axis.

Then we try to further improve the design, that is, further enhance the field strength in the loop center. We have the expression of rms current through the inductor:

$$I_{ac} = \sqrt{(\bar{n} + 1/2)\hbar\omega_0 / L_{tot}} \tag{4}$$

of which n is the average photon number. Thus, we have to reduce the total inductance L_{tot}. Which consists of loop wire inductance, stray inductance of capacitor, and kinetic inductance, which is not taken into account here.
First, we tried to adjust the loop geometry. We tried to make the radius smaller, shorten or longer the wires, change the circular shape to rectangular ones, and try double loops. However, the field in loop center does not change much.
Simulation using Ansys Maxwell shows that at 6 GHz, loop inductance is around 60 pH, but stray inductance is on the order of 300 pH. It may seems weird at first, why the interdigital capacitor tend to have a large stray inductance and largely affect our expected current through loop? This is because the adjacent digits have opposite polarities and are connected to terminals on opposite sides of the structure, ac current in adjacent digits flows in the same direction, creating inductance between the digits. [18]

2.2 Parallel plate design

To reduce this number, we figure out a parallel plate design [19], with superconducting loop penetrating the oxide thinfilm and connecting both planes, which provides large capacitance, and stray inductance as low as 30 pH at the same time.
To estimate the number of spins coupled to the resonator, we first plotted out the magnetic field distribution inside the loop, showing field strength as large as 152 nT in the center. With Er^{3+} doping density of 1.5 ppb, we could apply a Python code, plug in the equation to get a spin-resonator coupling strength of 14.6 kHz. And the number of ions been addressed is approximately 962.
However, not all of these spins contribute to the ultimate ESR signal. Taking into account the inhomogeneous broadening $1/T_2{}^*$ of Er spins, the ensemble spin linewidth (around

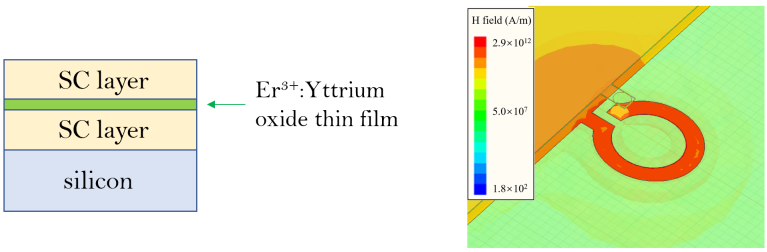

Figure 9: **Device structure of parallel plate design.** An erbium doped yttrium oxide thin film is sandwiched between the superconducting layers, deposited on silicon substrate. A loop is patterned on the lower layer, and is penetrated through a superconducting via and connected to the upper layer.

150 MHz) is much broader than the resonator linewidth (0.54 MHz). The ratio of spins contributing to the total signal is given by integration in frequency domain:

$$\epsilon = \int \rho_{LC}(\omega)\rho_{ESR}(\omega)d\omega \tag{5}$$

where $\rho_{LC} = 1/(1 + 4(\omega - \omega_0)^2/\kappa^2)$ is the ESR resonator spectral response and ρ_{ESR} is the spins density profile [12].

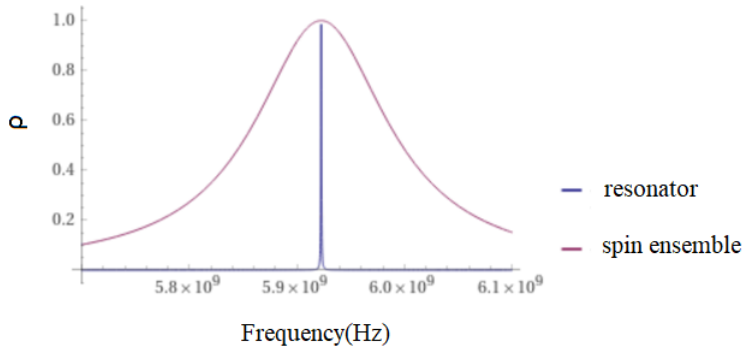

Figure 10: **Estimation of the number of spins contributing to total signal.**

Shown in Fig 10 is an illustration of spin density profile and resonator linewidth in our device. My brief calculation gives that the ratio is around 0.05, and this leads to the number of spins contributing to total signal: 962*0.047 ≈ 5. Single spin cooperativity is:

$$C_{singlespin} = \frac{4 \times (14.6\ kHz)^2}{(100\ kHz)(540\ kHz)} = 0.016 \tag{6}$$

This result shows that, using parallel plate resonator design, with around 152 nT magnetic field in the loop center, it would be promising to achieve single spin coupling and readout at low temperatures. In the future, we would perform more numeric simulations to look into methods of engineering cooperativity, and set up coherent readout protocols to reach the ultimate aim of single spin coupling and readout at milli-Kelvin temperatures [2].

2.3 Etched disk design

Since it is still unclear how to fabricate this parallel plate device, we work on the original on-chip design and put it into experiment.
However, due to the oxide dielectric loss and possible defects on the surface, the quality factor would be largely affected in real experiment. Instead of 1.1×10^4 as predicted Q, the quality factor is only on the order of hundreds in real measurement.
We have to perform further simulations since the original simulation result did not take into account of oxide thin film above silicon substrate. We should adjust parameters to find out the loss tangent of Yttrium oxide which could generate hundreds of Q for the resonator, and figure out ways to enhance Q.
As is shown in Fig 11, with a loss tangent of 1×10^{-2}, the resonator has a mode around 5.79 GHz with magnetic current confined in the loop, and has a quality factor around 600. This means Yttrium oxide thin film in real experiment is possible to have a loss tangent close to 1×10^{-2}.

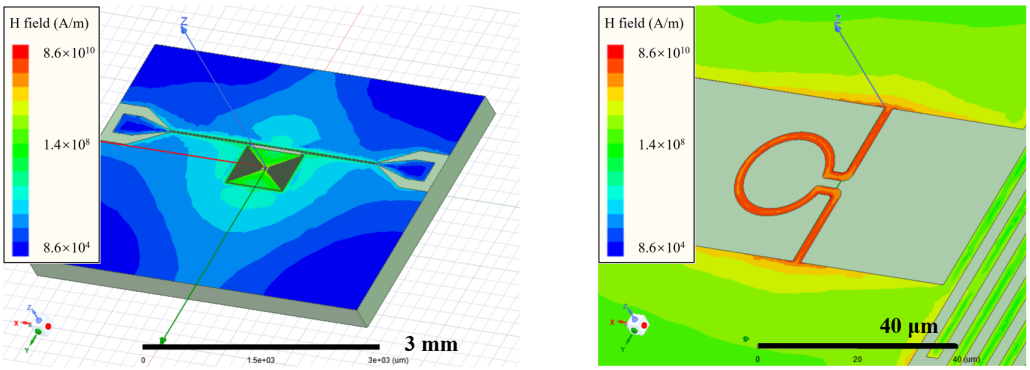

Frequency (GHz)	Q
5.79063+j 0.00487926	593.393

Figure 11: **Simulation result of resonator on a lossy oxide thin film**

To enhance quality factor of resonator, we think up an etching method. Since the loss from oxide is mainly from interaction of the EM field from above superconducting wires with the underneath oxide thin film, we could etch out the redundant part of the oxide thin film, only remaining the part within the loop, since we only need this circular part within the mode volume.
As is shown in Fig 12, the quality factor of resonator is enhanced to 2.1×10^8 for the etched disk design. This means that in real experiment, we could apply this etching method to achieve "good cavity", enhancing the quality factor thus getting a sharper resonance peak and higher sensitivity.
It is also intriguing to analyze the possible modes for the resonator. Except for the loop mode shown in above discussions, there would be another box mode around 7.4 GHz.
Overall, our simulation shows that the on-chip superconducting *LC* resonator has a loop mode around 6 GHz and a box mode around 7.5 GHz. And it is promising to use etching method to avoid oxide dielectric loss and achieve high quality factor. We also carried out simulations on a parallel plate design which shows potential for single spin coupling and readout at milli-Kelvin temperatures.

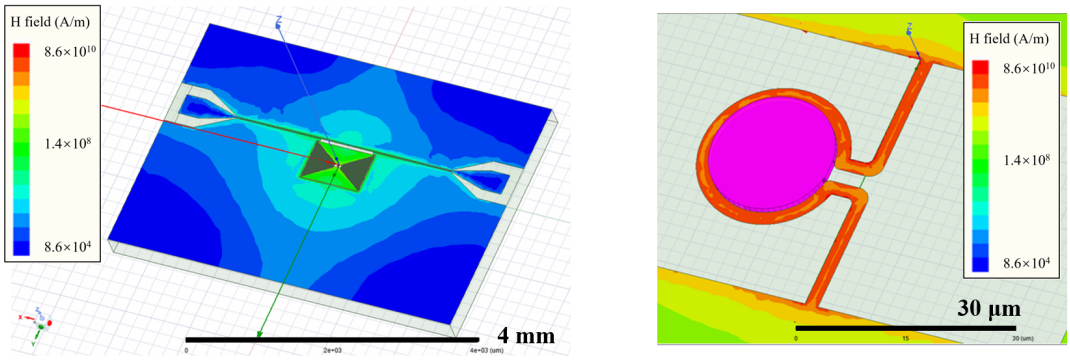

Frequency (GHz)	Q
5.90134+j 1.39475e-08	2.11556e+08

Figure 12: **Simulation result of resonator with disk shape oxide part**

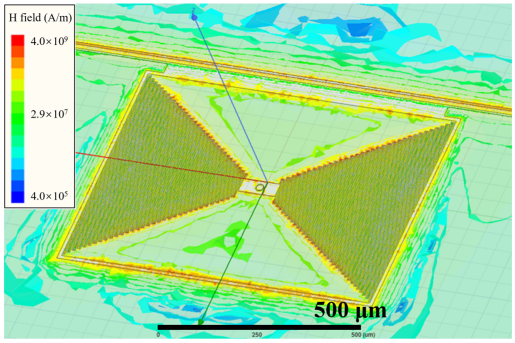

Frequency (GHz)	Q
7.44332 +j 0.00212553	1750.93

Figure 13: **Simulation of box mode at 7.44 GHz**

2.4 Experimental results

Shown in Fig 14 is an optical microscopy image of on-chip *LC* resonator, the fabrication process flow includes substrate cleaning, Nb deposition, photoresist coating, lithography, plasma etching, photoresist removing etc.

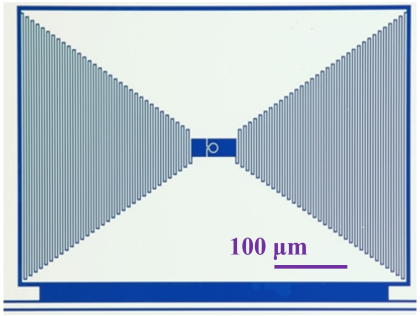

Figure 14: **Optical microscopy image of on-chip LC resonator**

We put the device in a custom designed chip holder, and connect both ports all the way out the fridge to a vector network analyzer (VNA). Then we cool down the device and collect the S_{21} parameter response (reflection coefficient).

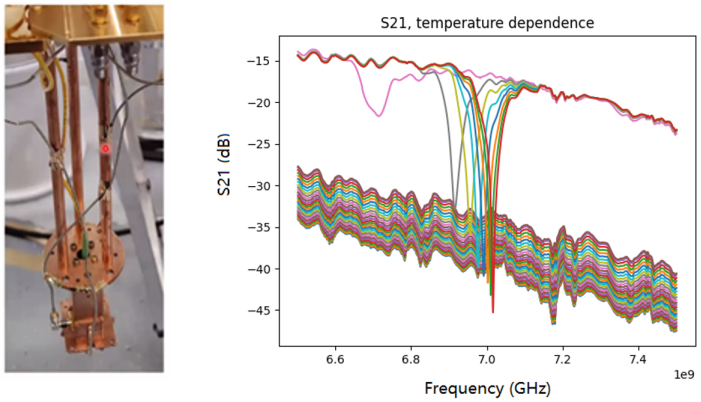

Figure 15: **S parameter response of on-chip resonator**

As is shown in Fig 16, the resonator feature: resonance peak appears below 9 K, which is the Niobium critical temperature. A fitting plot shows that the resonance is around 7.0 GHz, with quality factor around 200.
Different from what we expected, the resonance peak around 5.5 GHz, which is the loop mode, does not show obvious parallel magnetic field dependance and the data is not shown here. The reason for this phenomenon is still under investigation, we could compare our results with a similar work in [20].

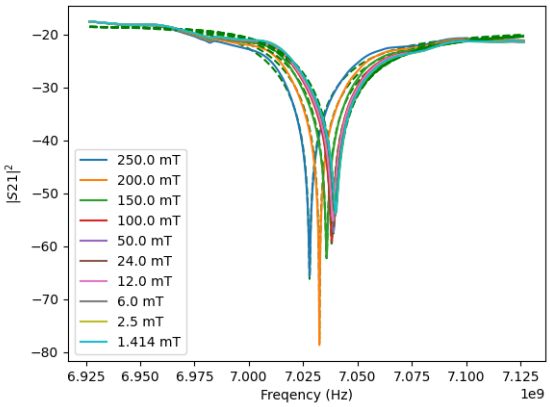

Figure 16: **Parallel magnetic field dependance of resonance feature.**

As is shown in Fig 16, the resonance feature around 7 GHz shows observable parallel magnetic field dependance and the resonance frequency decreases quadratically with field. What we expect is that, with applied external magnetic field, the spins coupled to the resonator will be polarized and will damp the original resonator field, which causes shifting of resonance features. So, the shifting response means that the resonator field is somehow coupled to the Erbium ions in the oxide layers, though simulation shows that this resonance mode is a box mode with fringing field, which is not meant to be coupled to the spins. We do need to carry out more simulations and experiments to confirm the

exact performance and field distribution of each mode.
In the future, we'd combine the device with state of art readout protocols. We'd perform pulsed ESR experiments, to estimate the coupling and reach higher signal to noise ratio.

3 Conclusion and discussion

Overall, we designed and simulated the performance of two kinds of nano-fabricated superconducting resonators. The parallel plated design shows potential of realizing single spin coupling and readout at milli-Kelvin temperatures, but the device is not fabricated and we have not carried out experiments. The on-chip LC resonator design is fabricated and put into experiment, but the resonance feature is different from what we expected and needs further investigation.
Still, the on-chip LC resonator device already shows clear resonance features and obvious dependance on external magnetic field, which are possible signs for coupling with spins. Also, we already come up with ways to improve its quality factor: etching out the redundant part of oxide layer and only remaining the disk part. In this way, we could get a better cavity with higher quality factor and it might show clearer response to our controlled fields and pulses, which is convenient for follow-up experiments.
In the future, we would find out more ways to engineer spin linewidth and enhance single spin cooperativity, and design robust readout chains to carry out more experiments. After carrying out ESR experiments and get stable coupling with Er spins, and after we optimize all the setup and protocols and get all the related parameters for spins in this system, we would apply laser to polarize the spins and reach more profound transduction aims.

References

[1] T. Zhong, J. M. Kindem, J. G. Bartholomew, J. Rochman, I. Craiciu, V. Verma, S. W. Nam, F. Marsili, M. D. Shaw, A. D. Beyer, and A. Faraon, "Optically addressing single rare-earth ions in a nanophotonic cavity," *Phys. Rev. Lett.*, vol. 121, p. 183603, Oct 2018. [Online]. Available: https://link.aps.org/doi/10.1103/PhysRevLett.121.183603

[2] P. Haikka, Y. Kubo, A. Bienfait, P. Bertet, and K. Mølmer, "Proposal for detecting a single electron spin in a microwave resonator," *Phys. Rev. A*, vol. 95, p. 022306, Feb 2017. [Online]. Available: https://link.aps.org/doi/10.1103/PhysRevA.95.022306

[3] T. Zhong, J. M. Kindem, J. G. Bartholomew, J. Rochman, I. Craiciu, E. Miyazono, M. Bettinelli, E. Cavalli, V. Verma, S. W. Nam, F. Marsili, M. D. Shaw, A. D. Beyer, and A. Faraon, "Nanophotonic rare-earth quantum memory with optically controlled retrieval," *Science*, vol. 357, no. 6358, pp. 1392–1395, 2017. [Online]. Available: https://science.sciencemag.org/content/357/6358/1392

[4] L. A. Williamson, Y.-H. Chen, and J. J. Longdell, "Magneto-optic modulator with unit quantum efficiency," *Phys. Rev. Lett.*, vol. 113, p. 203601, Nov 2014. [Online]. Available: https://link.aps.org/doi/10.1103/PhysRevLett.113.203601

[5] C. Eichler, A. J. Sigillito, S. A. Lyon, and J. R. Petta, "Electron spin resonance at the level of 10^4 spins using low impedance superconducting resonators," *Phys. Rev. Lett.*, vol. 118, p. 037701, Jan 2017. [Online]. Available: https://link.aps.org/doi/10.1103/PhysRevLett.118.037701

[6] C. Thiel, T. Böttger, and R. Cone, "Rare-earth-doped materials for applications in quantum information storage and signal processing," *Journal of Luminescence*, vol. 131, no. 3, pp. 353–361, 2011, selected papers from DPC'10. [Online]. Available: https://www.sciencedirect.com/science/article/pii/S002223131000534X

[7] M. K. Singh, A. Prakash, G. Wolfowicz, J. Wen, Y. Huang, T. Rajh, D. D. Awschalom, T. Zhong, and S. Guha, "Epitaxial er-doped y2o3 on silicon for quantum coherent devices," *APL Materials*, vol. 8, no. 3, p. 031111, 2020. [Online]. Available: https://doi.org/10.1063/1.5142611

[8] N. Ohlsson, "Quantum optics and quantum information processing in rare-earth-ion-doped crystals," Ph.D. dissertation, Atomic Physics, 2003.

[9] S. Probst, H. Rotzinger, S. Wünsch, P. Jung, M. Jerger, M. Siegel, A. V. Ustinov, and P. A. Bushev, "Anisotropic rare-earth spin ensemble strongly coupled to a superconducting resonator," *Phys. Rev. Lett.*, vol. 110, p. 157001, Apr 2013. [Online]. Available: https://link.aps.org/doi/10.1103/PhysRevLett.110.157001

[10] M. Zhong, R. L. A. Morgan P. Hedges, S. E. B. John G. Bartholomew, J. J. L. Sven M. Wittig, and M. J. Sellars, "Optically addressable nuclear spins in a solid with a six-hour coherence time," *Nature*, vol. 517, pp. 177–180, 2015. [Online]. Available: https://www.nature.com/articles/nature14025#citeas

[11] M. Ranvci'c, M. Hedges, R. Ahlefeldt, and M. Sellars, "Coherence time of over a second in a telecom-compatible quantum memory storage material," *Nature Physics*, vol. 14, pp. 50–54, 2018.

[12] A. Bienfait, "Magnetic resonance with quantum microwaves," Ph.D. dissertation, Université Paris-Saclay, 3 2017, nNT :2016SACLS297ff.

[13] X. R. Wang, Y. S. Zheng, and S. Yin, "Spin relaxation and decoherence of two-level systems," *Phys. Rev. B*, vol. 72, p. 121303, Sep 2005. [Online]. Available: https://link.aps.org/doi/10.1103/PhysRevB.72.121303

[14] "Two state quantum system." Website, 20 October 2020, at 07:13 (UTC), https://en.wikipedia.org/wiki/Spin_echo.

[15] A. Bienfait, Y. K. J. J. Pla, X. Z. M. Stern, C. D. W. C. C. Lo, M. L. W. T. T. Schenkel, D. E. D. Vion, K. M. B. Julsgaard, J. J. L. Morton, and P. Bertet, "Reaching the quantum limit of sensitivity in electron spin resonance," *Nature Nanotech*, vol. 11, p. 253–257, 2016. [Online]. Available: https://www.nature.com/articles/nnano.2015.282#citeas

[16] Y. Kubo, F. R. Ong, P. Bertet, D. Vion, V. Jacques, D. Zheng, A. Dréau, J.-F. Roch, A. Auffeves, F. Jelezko, J. Wrachtrup, M. F. Barthe, P. Bergonzo, and D. Esteve, "Strong coupling of a spin ensemble to a superconducting resonator," *Phys. Rev. Lett.*, vol. 105, p. 140502, Sep 2010. [Online]. Available: https://link.aps.org/doi/10.1103/PhysRevLett.105.140502

[17] Y. Twig, E. Suhovoy, and A. Blank, "Sensitive surface loop-gap microresonators for electron spin resonance," *Review of Scientific Instruments*, vol. 81, no. 10, p. 104703, 2010. [Online]. Available: https://doi.org/10.1063/1.3488365

[18] S. Edward, "Interdigital capacitor with selfcanceling inductance," Jul 2010.

[19] B. Sarabi, P. Huang, and N. M. Zimmerman, "Possible hundredfold enhancement in the direct magnetic coupling of a single-atom electron spin to a circuit resonator," *Phys. Rev. Applied*, vol. 11, p. 014001, Jan 2019. [Online]. Available: https://link.aps.org/doi/10.1103/PhysRevApplied.11.014001

[20] L. McKenzie-Sell, J. Xie, C.-M. Lee, J. W. A. Robinson, C. Ciccarelli, and J. A. Haigh, "Low-impedance superconducting microwave resonators for strong coupling to small magnetic mode volumes," *Phys. Rev. B*, vol. 99, p. 140414, Apr 2019. [Online]. Available: https://link.aps.org/doi/10.1103/PhysRevB.99.140414